International Journal of Thermophysics, Vol. 13, No. 6, 1992

Thermal Conductivity of the New Refrigerants R134a, R152a, and R123 Measured by the Transient Hot-Wire Method

U. Gross,[1] Y. W. Song,[1] and E. Hahne[1]

Received May 29, 1992

Thermal-conductivity measurements are reported for the new refrigerants R134a, R152a und R123. Transient hot-wire experiments were performed which cover both the liquid and vapor states at temperatures and pressures ranging from $\vartheta = -20°C$ to 90°C and from $p = 0.1$ bar to 60 bar respectively. The results are correlated with density and temperature. In addition temperature dependent correlations are presented for (i) saturated liquid, (ii) saturated vapor, (iii) ideal gas (which equals approximately vapor state at ambient pressure). Finally the results are compared with data from the literature and also with the thermal conductivities of R12 and R11.

KEY WORDS: refrigerants; R134a; R152a; R123; thermal conductivity; transient hot-wire method.

1. INTRODUCTION

R11 (CCl_3F) and R12 (CCl_2F_2) have been used in industry and households for about 50 years. Both substances will be replaced in the very near-future by, e.g., R123 ($CHCl_2$–CF_3) in the case of R11 and R134a (CF_3–CH_2F), R152a (CHF_2–CH_3), or a mixture of them in the case of R12.

In the present work thermal conductivities of R134a, R152a, and R123 were measured in the liquid state (saturated and subcooled) and in the vapor state (saturated and superheated). The ranges of temperature ($-20°C < \vartheta < 90°C$) and pressure ($1 < p < 60$ bar; for liquid R123, $0.1 < p < 60$ bar) cover all states of technical interest. The measurements

[1] Institut für Thermodynamik und Wärmetechnik, Universität Stuttgart, Pfaffenwaldring 6, 7000 Stuttgart 80, Germany.

0195-928X/92/1100-0957$06.50/0

were performed with a transient hot-wire method which is the current leading technique for measuring the thermal conductivity of fluids. The method has been described in numerous publications, e.g., Refs. 1–5, where both its theory and its practical application to various fluids are presented. Therefore a short description of the theoretical basis will suffice here.

2. THEORETICAL BASIS

The transient hot-wire method is based on the following principle. The fluid being considered is contained in a pressure vessel which is submerged in a temperature-controlled water bath. Before the measurements are started, the vessel and its contents are brought to thermal equilibrium at a given temperature T_0. At time $t=0$, an electric current is passed through a thin platinum wire ($r_w = 8.5\ \mu$m in the present experiments) inside the vessel, yielding a constant heat flux Q_1 per unit length. The temperatures of both the wire and the surrounding fluid begin to rise. During a short time interval ($t \leqslant 2$ s for the present measurements), heat is transported to the fluid by transient conduction and the wire temperature increases according to the thermal conductivity of the fluid. Later a natural convection flow will appear due to the increasing temperature differences within the fluid. The development of the temperature field around the wire during the conduction period is described by the following differential equation:

$$\rho c_p \frac{\partial T}{\partial t} = \lambda \left[\frac{1}{r} \frac{\partial T}{\partial r} + \frac{\partial^2 T}{\partial r^2} \right] \tag{1}$$

For an explanation of notation, see Nomenclature (below). After some simplifications the time history of the wire temperature, $T(t)$, is obtained from Eq. (1) by integration:

$$T = T_0 + \frac{Q_1}{4\pi\lambda} \ln \left[\frac{4at}{r_w^2 C} \right] \tag{2}$$

The temperature rise, ΔT, in our measurements is $\Delta T = 0.5$ to 1 K. The derivative of temperature with time (this is obtained by using the wire as a resistance thermometer) renders a simple equation for the thermal conductivity:

$$\lambda = \frac{Q_1/4\pi}{\partial T/\partial(\ln t)} \tag{3}$$

3. EXPERIMENTS

3.1. Experimental Setup

Figure 1 shows the measuring cell which has been successfully applied for a large number of thermal-conductivity measurements [6–13]. It is constructed as a pressure vessel (stainless steel) with two cylindrical boreholes ($d_i = 30$ mm). The boreholes are suitable as measuring chambers for many fluids without further modifications, but not for polar substances such as water and R134a. For such fluids special efforts have to be taken in order to minimize the strength of the electric field. In our experiments the fluids were contained together with the platinum heating wires and the connecting silver wires in glass tubes ($d_i = 27$ mm) which fitted into the boreholes. The silver wires were shrouded by a glass capillary. A cylinder

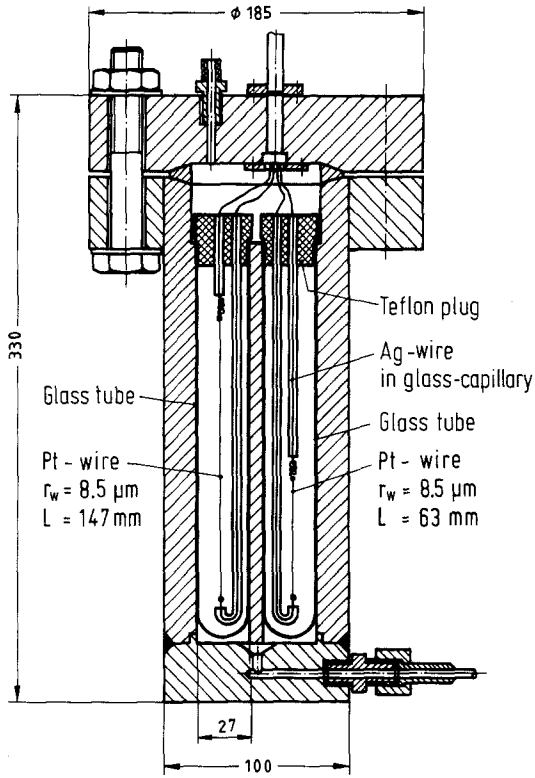

Fig. 1. Measuring cell.

with a plunger allowed for the variation of mass and accordingly density in the measuring cell. Pressures were indicated by a pressure transducer (Paroscientific; 0 to 62 bar; accuracy, ±6.2 mbar).

3.2. Test Fluids

The new refrigerants were selected for their low "ozone-depletion potential" (ODP) and low "global-warming potential" (GWP) as the leading criteria. The respective values are listed in Table I together with further relevant data. The refrigerant R123 was obtained with a commercial purity of 99.8%. According to the manufacturer's information, R123 contains about 2% of the isomere R123a and 0.2% of other substances. This information was not available for R152a, but its purity is given as 99.9%. The third substance, R134a, could also be obtained with a purity of 99.9% with the isomere R134 and water as the contaminants. Inert gases, which may possibly be absorbed in the test fluids, were removed by repeated solidification of the fluids, in liquid nitrogen, and extraction of the remaining gases.

3.3. Experimental Procedure and Accuracy of the Measurements

Prior to the experiments, the complete apparatus (measuring cell and plunger) was repeatedly evacuated and rinsed with the substance to be investigated. Finally, the apparatus was completely filled with the test fluid in the liquid state by distillation from the container.

The state of the fluid in the measuring cell could be changed by varying the temperature (of the water bath) and by varying the mean density in the apparatus by two different measures:

(i) variation of the total volume in the apparatus by means of the plunger, with the total mass of fluid remaining constant; or

(ii) or reduction of the fluid mass in the system.

Table I. Test Fluids

	Structure	Molar mass ($g \cdot mol^{-1}$)	Relative ODP	Relative GWP	ϑ_{triple} (°C)	$\vartheta_{n.b.}$ (°C)	ϑ_{crit} (°C)	p_{crit} (bar)	Supplied by	Purity (%)
R12	CCl_2F_2	120.92	1	1	−155	−29.8	112.0	41.6		
R134a	CF_3–CH_2F	102.03	0	0.09	−101	−26.1	101.1	40.6	ICI	99.9
R152a	CHF_2–CH_3	66.05	0	0.01	−117	−24.2	113.3	45.2	Solvay	99.9
R11	CCl_3F	137.38	1	0.4	−111	23.8	198.0	44.0		
R123	$CHCl_2$–CF_3	152.93	0.022	0.006	−107	27.9	183.8	36.7	Solvay	99.8

There are differences regarding the procedure in liquid and vapor states. A series of thermal-conductivity measurements of subcooled liquid along an isotherm starts at some high pressure (max. 60 bar); the pressure is then reduced step by step until the saturation state is attained. In the case of the vapor, a series of measurements along an isotherm starts at the lowest pressure (at about 1 bar) in the superheated state; the pressure is then gradually raised to the saturation state.

The precautions taken for polar fluids were tested with such well-investigated fluids as toluene and water. The results agree with the literature data with a maximum deviation of $\pm 1\%$. The protective measures proved to be sufficient for experiments with R152a und R123. Measurements with liquid R134a, however, turned out to be defective. As suggested by Ross et al. [14], a small electric potential (about 6 V) was applied between the platinum wire and the metal wall of the pressure vessel prior to and during the experiment. This resulted in a prepolarization of the fluid next to the wire, where the intensity of the electric field is largest. By this procedure, measurements with R134a became reproducible.

Principally the thermal conductivity of a fluid will be affected by the orientation of its molecules. Since, however, the thermal conductivity is determined as an average value for a comparatively large volume, the preorientation of some monolayers of molecules close to the wire is considered to be negligible. In a test with the protection voltage being reduced gradually to zero, it was found that reliable experiments without prepolarization can be performed in liquid R134a only at low temperatures ($\vartheta < 0°C$).

The accuracy of the measured thermal conductivity was analyzed thoroughly and maximum errors for liquids and vapors were found to remain within ± 1.6 and $\pm 2\%$, respectively. Uncertainties are due to deviations from the ideal mathematical model of a line source in the infinite space, effects of convection and radiation, limited accuracy of the Wheatstone bridge used for the measurements, and some additional effects as discussed in Ref. 3. Corrections were applied for differences between wire and fluid heat capacities and, also, for temperature-dependent variations of fluid properties and heat flux in the course of the experiment. Radiation effects were not considered, whereas outer boundary effects were checked to keep below 0.01%.

4. RESULTS

The measured thermal conductivities are listed in Tables II to IV, together with the temperature, pressure, and density values. The density

Table II. Density and Thermal Conductivity of R134a

ϑ (°C)	p (bar)	ρ ($kg \cdot m^{-3}$)	λ ($W \cdot m^{-1} \cdot K^{-1}$)
−19.9	42.72	1360.0	0.10605
−19.9	1.35	1352.0	0.10474
−10.2	58.09	1342.0	0.10352
−10.2	42.90	1338.0	0.10170
−10.2	21.30	1334.0	0.10044
−10.2	2.01	1324.7	0.10059
0.0	59.22	1314.8	0.09835
0.0	25.05	1309.0	0.09592
0.0	15.52	1305.3	0.09502
0.0	2.92	1292.0	0.09509
10.1	60.97	1283.3	0.09462
10.1	42.03	1275.8	0.09322
10.1	23.23	1267.5	0.09146
10.1	4.17	1258.5	0.09066
20.0	56.50	1249.7	0.09033
20.0	33.57	1237.7	0.08815
20.0	17.17	1228.0	0.08756
20.0	5.74	1223.9	0.08618
30.0	60.25	1218.3	0.08600
30.0	36.48	1204.8	0.08451
30.0	22.45	1196.2	0.08355
30.2	7.76	1186.0	0.08186
40.0	58.19	1181.6	0.08246
40.0	42.05	1171.6	0.08075
40.0	26.92	1161.8	0.07944
40.0	10.33	1146.9	0.07743
50.0	59.50	1143.7	0.07874
50.0	39.60	1129.5	0.07716
50.0	25.20	1117.6	0.07612
50.0	15.80	1109.1	0.07346
50.0	13.10	1107.6	0.07301
60.1	57.50	1099.1	0.07410
60.1	39.20	1087.2	0.07302
60.1	25.10	1064.8	0.07011
60.0	16.71	1055.3	0.06969
70.2	57.20	1050.2	0.06932
70.2	40.10	1028.7	0.06738
70.2	24.77	998.6	0.06521
70.2	20.89	993.3	0.06491
80.3	57.06	995.2	0.06510
80.3	43.00	971.6	0.06334
80.3	30.29	936.2	0.06219
80.3	26.29	930.4	0.06156

Table II. (*Continued*)

ϑ (°C)	p (bar)	ρ (kg·m^{-3})	λ (W·m^{-1}·K^{-1})
90.0	56.08	934.2	0.06132
90.0	43.60	904.6	0.06024
90.0	33.30	863.9	0.05759
0.6	2.90	14.28	0.01206
0.6	2.76	13.50	0.01224
0.6	1.76	8.31	0.01205
21.0	5.67	27.58	0.01396
21.0	5.66	27.23	0.01381
21.0	3.76	17.19	0.01340
21.0	3.46	15.68	0.01352
21.0	2.96	13.23	0.01341
21.0	2.46	10.86	0.01320
21.0	1.76	7.65	0.01298
21.0	0.96	4.09	0.01306
41.5	10.12	49.83	0.01673
41.5	9.56	45.88	0.01641
41.5	9.36	45.00	0.01653
41.5	9.16	43.74	0.01644
41.5	8.96	42.22	0.01600
41.5	7.96	36.50	0.01605
41.5	6.96	31.13	0.01557
41.5	5.96	26.04	0.01550
41.5	3.56	14.79	0.01493
41.5	0.96	3.80	0.01496
50.8	0.96	3.69	0.01575
60.8	16.56	85.12	0.02012
60.8	14.96	73.26	0.01926
60.8	12.96	59.97	0.01843
60.8	10.96	48.40	0.01787
60.8	8.96	37.97	0.01752
60.8	6.96	28.42	0.01727
60.8	4.96	19.58	0.01676
60.8	1.96	7.40	0.01671
60.8	0.96	3.57	0.01637
81.0	25.85	148.00	0.02464
81.0	21.96	109.39	0.02260
81.0	19.96	94.27	0.02182
81.0	17.96	80.96	0.02094
81.0	15.96	69.11	0.02021
81.0	13.96	58.26	0.01955
81.0	9.96	39.01	0.01860
81.0	7.96	30.33	0.01857
81.0	5.96	22.12	0.01848
81.0	3.96	14.38	0.01769
81.0	1.96	6.21	0.01784

Table III. Density and Thermal Conductivity of R152a

ϑ (°C)	p (bar)	ρ (kg · m^{-3})	λ (W · m^{-1} · K^{-1})
−19.9	4.99	1003.0	0.12859
−19.9	1.76	1002.4	0.12687
−10.0	51.75	992.0	0.12630
−9.9	44.60	990.3	0.12558
−9.9	22.60	985.5	0.12391
−9.8	1.82	980.6	0.12179
0.0	59.52	972.8	0.12123
0.0	46.15	969.7	0.12091
0.0	21.70	963.8	0.11848
0.0	5.26	959.6	0.11763
0.2	2.65	958.5	0.11720
10.1	60.34	951.4	0.11594
10.1	51.35	949.0	0.11526
10.1	32.50	933.9	0.11312
10.1	14.80	938.9	0.11173
10.1	3.73	935.7	0.11176
20.0	62.05	929.9	0.11190
20.0	47.10	925.5	0.10960
20.0	29.42	919.9	0.10842
20.0	12.00	914.2	0.10750
19.8	5.09	912.3	0.10698
30.0	62.20	906.9	0.10633
30.0	30.96	895.9	0.10418
30.0	15.16	889.9	0.10287
30.0	6.87	886.5	0.10219
40.0	60.44	882.0	0.10219
40.0	43.59	875.2	0.09985
40.0	25.26	867.3	0.09841
40.0	9.07	859.1	0.09720
50.0	61.65	846.1	0.09710
50.0	42.60	840.6	0.09559
50.0	24.68	834.3	0.09373
50.0	11.76	830.0	0.09262
60.0	59.00	817.4	0.09262
60.0	40.38	809.8	0.09096
60.0	23.62	805.9	0.08946
70.0	59.00	787.2	0.08852
70.0	42.55	779.5	0.08681
70.0	23.33	772.5	0.08407
80.0	61.42	757.3	0.06452
80.0	46.31	747.3	0.08350
80.0	33.00	738.9	0.08078

Table III. (*Continued*)

ϑ (°C)	p (bar)	ρ (kg·m^{-3})	λ (W·m^{-1}·K^{-1})
90.0	53.44	714.5	0.07867
90.0	39.00	699.8	0.07652
−18.8	1.21	3.97	0.01093
−18.8	0.75	2.41	0.01069
0.9	2.62	8.26	0.01271
0.9	0.82	2.43	0.01215
20.8	5.12	15.86	0.01459
20.8	3.64	10.79	0.01423
20.8	2.47	7.10	0.01410
20.8	0.88	2.43	0.01388
40.8	9.05	28.15	0.01715
40.8	8.08	24.51	0.01664
40.8	7.01	20.57	0.01649
40.8	5.93	16.95	0.01618
40.8	4.45	12.33	0.01604
40.8	2.67	7.12	0.01569
40.8	0.94	2.44	0.01546
60.7	14.76	47.24	0.02011
60.7	13.67	41.87	0.01949
60.7	12.69	38.24	0.01907
60.7	10.72	30.79	0.01840
60.7	8.93	24.68	0.01810
60.7	7.58	20.39	0.01800
60.7	6.10	15.97	0.01764
60.7	4.91	12.61	0.01749
60.7	2.86	7.12	0.01717
60.7	0.99	2.40	0.01702
80.7	22.53	76.11	0.02437
80.7	21.89	72.27	0.02383
80.7	20.60	65.86	0.02323
80.7	19.95	62.14	0.02286
80.7	18.09	53.76	0.02223
80.7	16.61	47.72	0.02143
80.7	14.89	41.35	0.02120
80.7	12.77	34.11	0.02080
80.7	11.44	29.90	0.02040
80.7	9.64	24.51	0.01990
80.7	8.21	20.52	0.01953
80.7	6.49	15.77	0.01951
80.7	5.13	12.81	0.01937
80.7	3.06	7.12	0.01908
80.7	1.05	2.39	0.01895

Table IV. Density and Thermal Conductivity of R123

ϑ (°C)	p (bar)	ρ ($kg \cdot m^{-3}$)	λ ($W \cdot m^{-1} \cdot K^{-1}$)
−19.0	41.45	1576.3	0.09161
−19.0	21.13	1572.5	0.09093
−19.6	0.13	1570.2	0.09030
−9.6	61.82	1559.3	0.08956
−9.6	39.90	1555.0	0.08886
−9.6	20.27	1551.1	0.08812
−9.6	0.24	1547.0	0.08744
0.5	61.18	1536.8	0.08741
0.5	39.97	1532.2	0.08623
0.4	20.26	1527.9	0.08563
0.6	0.36	1523.4	0.08475
10.7	51.56	1511.8	0.08385
10.7	40.64	1509.2	0.08335
10.3	19.75	1504.1	0.08282
10.7	0.55	1499.4	0.08180
20.7	62.27	1491.2	0.08161
20.4	40.87	1485.7	0.08077
21.0	18.97	1479.8	0.07979
20.5	0.75	1474.8	0.07904
30.8	61.05	1467.3	0.07862
30.4	39.54	1461.2	0.07782
31.1	20.42	1455.5	0.07705
30.8	1.10	1449.6	0.07625
40.6	55.35	1441.5	0.07580
40.6	17.35	1429.1	0.07408
40.3	1.55	1423.7	0.07319
50.6	61.19	1418.6	0.07353
50.4	40.12	1411.2	0.07259
50.6	20.81	1404.1	0.07155
50.3	2.14	1396.9	0.07075
60.7	61.85	1393.5	0.07100
60.7	40.20	1385.0	0.07008
60.6	21.18	1377.1	0.06900
60.5	2.86	1369.2	0.06820
70.7	61.37	1367.2	0.06866
70.7	37.72	1356.7	0.06709
70.7	19.19	1348.1	0.06585
70.4	3.81	1340.5	0.06506

Table IV. (*Continued*)

ϑ (°C)	p (bar)	ρ (kg · m^{-3})	λ (W · m^{-1} · K^{-1})
80.7	61.15	1340.2	0.06566
80.8	40.73	1330.0	0.06495
80.8	19.85	1319.1	0.06354
80.3	4.94	1310.7	0.06269
31.3	1.00	6.36	0.01062
31.6	1.00	6.36	0.01056
31.9	1.00	6.34	0.01050
41.2	1.39	8.68	0.01122
41.2	1.19	7.37	0.01114
41.3	1.00	6.13	0.01106
51.2	2.10	12.92	0.01204
51.2	1.50	9.00	0.01184
51.2	1.02	5.99	0.01178
61.4	2.73	16.50	0.01239
61.2	2.51	15.07	0.01233
61.3	2.03	11.95	0.01237
61.4	1.54	8.93	0.01231
61.2	1.02	5.79	0.01222
71.1	3.63	21.73	0.01309
71.3	2.92	17.09	0.01284
71.1	2.43	13.98	0.01282
71.4	1.97	11.19	0.01276
71.0	1.03	5.68	0.01273
81.1	4.74	28.24	0.01361
81.2	4.53	26.79	0.01353
81.2	3.87	22.42	0.01333
81.3	2.83	15.89	0.01333
81.3	2.08	11.42	0.01313
81.4	1.02	5.48	0.01314
91.4	5.94	35.21	0.01416
91.2	4.93	28.30	0.01405
91.2	3.49	19.24	0.01390
91.2	3.01	16.39	0.01386
91.3	2.26	12.07	0.01382
91.3	1.74	9.17	0.01376
91.4	1.03	5.34	0.01373

was calculated from respective equations of state for R134a [15], R152a (liquid [16] and vapor [17]), and R123 [15].

4.1. Thermal Conductivity of R134a

The thermal conductivity of fluid substances is usually plotted as a function of density, and a monotonuously increasing curve is obtained if states far away from the critical point are considered. Figure 2 shows such a diagram of our results for R134a and some literature data. The thermal conductivity of R134a is found to behave in the expected way, with a significant density effect and a nonvanishing conductivity at zero density (i.e., for the ideal gas). Around the critical density, the well-known enhancement of the thermal conductivity is represented by dashed supercritical isotherms. The ranges of liquid (high density) and vapor (low density) which are of practical interest are indicated by the two dashed rectangles, and they are replotted in Figs. 3 and 4 on an enlarged scale. These more detailed presentations show an additional temperature effect, which is dominating for vapors (Fig. 4) but is very small for liquids (Fig. 3). The measured results can be correlated with temperature and density by the following polynomial expression:

$$\lambda(\vartheta, \rho) = a_0 + a_1\vartheta + a_2\rho + a_3\rho^2 + a_4\rho^3 + a_5\rho^4 \tag{4}$$

Equation (4) was fitted to the total number of the measured results (88 data points) by two-dimensional regression. The coefficients a_i are included

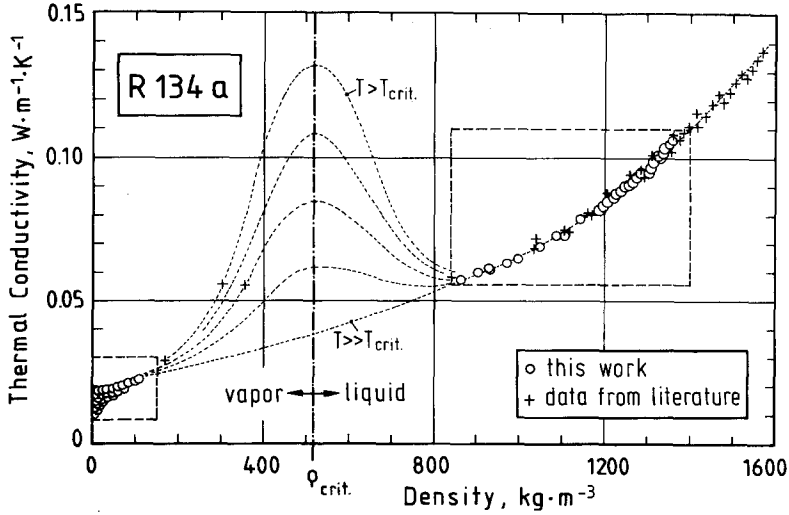

Fig. 2. Thermal conductivity of R134a as a function of density.

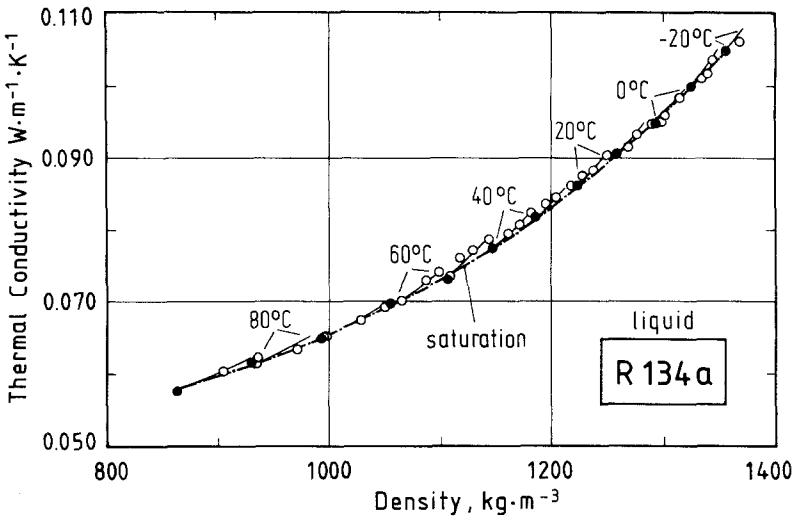

Fig. 3. Density and temperature effects on the thermal conductivity of R134a (liquid phase).

in Table V, where additional information about the range of application and deviations between correlation and data points is listed. Equation (4) represents the so-called "background conductivity"; it cannot describe the enhancement of the thermal conductivity around the critical point. An additional term is required when this effect is to be accounted for; see

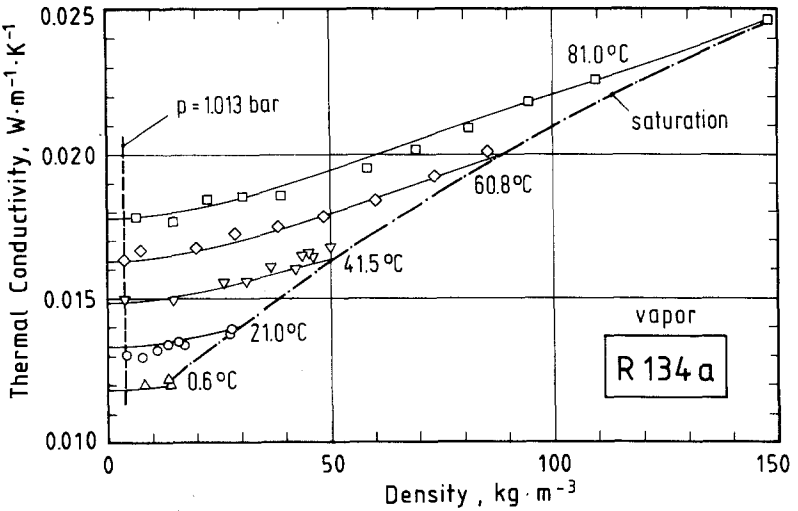

Fig. 4. Density and temperature effects on the thermal conductivity of R134a (vapor phase).

Table V. Coefficients in Eq. (4): $\lambda(\vartheta, \rho) = a_0 + a_1\vartheta + a_2\rho + a_3\rho^2 + a_4\rho^3 + a_5\rho^4$ with λ in $W \cdot m^{-1} \cdot K^{-1}$, ϑ in °C, and ρ in $kg \cdot m^{-3}$

	R134a	R152a	R123
a_0	0.0113853	0.0118907	0.0089825
a_1	0.754957×10^{-4}	0.799882×10^{-4}	0.548136×10^{-4}
a_2	0.409834×10^{-4}	0.680531×10^{-4}	-0.488536×10^{-5}
a_3	0.215976×10^{-7}	0.634900×10^{-7}	0.457510×10^{-7}
a_4	$-0.515103 \times 10^{-10}$	-0.166287×10^{-9}	$-0.319674 \times 10^{-10}$
a_5	0.378355×10^{-13}	0.151694×10^{-12}	0.167167×10^{-13}
	Range of application		
Temperature	−20 to 90°C	−20 to 90°C	−20 to 90°C
Pressure	1 to 60 bar	1 to 60 bar	0.1 to 60 bar
	Number of data points and deviation from the suggested correlation		
Number	88	84	74
Mean dev.	0.9%	0.7%	0.6%
Max. dev.	3.1%	2.6%	2.6%

Ref. 6. In the subcritical range, however, for $(\vartheta_{crit} - \vartheta) > 10$ K, the enhancement is not significant.

Figure 3 shows results for liquid R134a, with filled and open symbols representing saturated and subcooled states, respectively. Isotherms are indicated by solid-line curves, whereas saturation states are interconnected by the thicker dashed-dotted line. Figure 4 shows the results for R134a vapor along five isotherms between $\vartheta = 0.6$°C and $\vartheta = 81.0$°C at pressures between ambient and saturation. In order to improve the correlation, especially for the dilute gas ($\rho = 0$), a two-dimensional regression was performed for the results in the vapor state only (with 42 data points). This correlation is presented as Eq. (5), and coefficients b_i are given in Table VI.

$$\lambda(\vartheta, \rho) = b_0 + b_1\vartheta + b_2\rho + b_3\rho^2 + b_4\rho^3 + b_5\rho^4, \qquad \text{with} \quad b_2 = 0! \qquad (5)$$

By setting $b_2 = 0$, Eq. (5) contains no linear term in density and thus the density effect on thermal conductivity is strongly reduced close to the ideal-gas state ($\rho \to 0$); at this state the density effect should vanish according to the kinetic theory of gases.

Equation (5) permits the determination of thermal conductivities of both superheated gas (solid-line curves in Fig. 4) and gas at saturation state (dashed-dotted line). The dashed line in Fig. 4 connecting states at ambient pressure meets the saturation state at the normal boiling point

Table VI. Coefficients in Eqs. (5) and (8): $\lambda(\vartheta, \rho) = b_0 + b_1\vartheta + b_2\rho + b_3\rho^2 + b_4\rho^3 + b_5\rho^4$, with λ in $W \cdot m^{-1} \cdot K^{-1}$, ϑ in °C, and ρ in $kg \cdot m^{-3}$

	R134a	R152a	R123
b_0	0.0117958	0.0122641	0.0090535
b_1	0.739399×10^{-4}	0.813494×10^{-4}	0.501649×10^{-4}
b_2	0.0	0.0	0.0
b_3	0.103736×10^{-5}	0.270862×10^{-5}	0.199345×10^{-5}
b_4	-0.851602×10^{-8}	-0.441888×10^{-7}	-0.811145×10^{-7}
b_5	0.244985×10^{-10}	0.278126×10^{-9}	0.104170×10^{-8}
	Range of application		
Temperature	0 to 80°C	−20 to 80°C	30 to 90°C
Pressure	1 to 26 bar	1 to 23 bar	1 to 6 bar
	Number of data points and deviation from the suggested correlation		
Number	42	40	32
Mean dev.	1.0%	0.7%	0.5%
Max. dev.	3.2%	1.8%	1.9%

($\vartheta_{n.b.} = -26.1$°C). It was found that vapors at $p = 1.013$ bar may be regarded as ideal gases with respect to thermal conductivity.

For practical calculations, the thermal conductivities in the saturation states (liquid and vapor), as well as in the vapor state at ambient pressure ($p = 1.013$ bar), are of special interest. These thermal conductivities are plotted versus temperature in Fig. 5. Here no extrapolation along isotherms was required, as our measurements included all the relevant pressure and temperature ranges. Three solid lines, labeled λ', λ'', and λ_0, correlate our data.

For the saturated liquid,

$$\lambda'(\vartheta) = c_0 + c_1\vartheta \tag{6}$$

For the saturated vapor,

$$\lambda''(\vartheta) = d_0 + d_1\vartheta + d_2\vartheta^2 \tag{7}$$

And for vapor at ambient pressure, according to Eq. (5) when the ideal-gas conductivity is assumed by setting $\rho = 0$,

$$\lambda_0(\vartheta) = b_0 + b_1\vartheta \tag{8}$$

The coefficients b_i, c_i, and d_i are listed in Tables VI to VIII. Again, it can be seen in Fig. 5 that vapor thermal conductivities in the ambient (λ_0) and

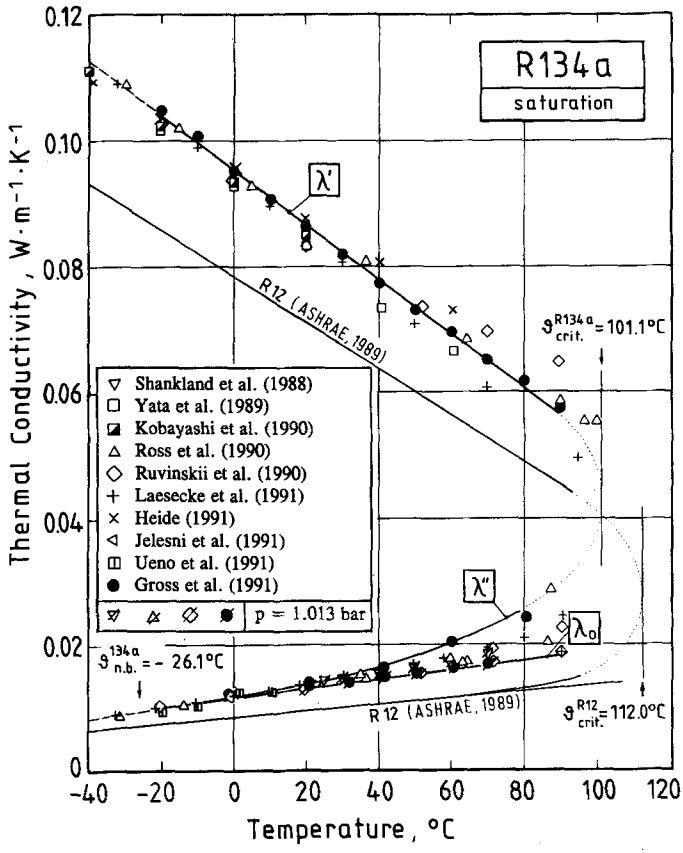

Fig. 5. Thermal conductivity of R134a in the saturated liquid and vapor states.

Table VII. Coefficients in Eq. (6): $\lambda'(\vartheta) = c_0 + c_1\vartheta$ with λ' in $W \cdot m^{-1} \cdot K^{-1}$ and ϑ in °C

	R134a	R152a	R123
c_0	0.095397	0.116747	0.0847822
c_1	-0.43478×10^{-3}	-0.46025×10^{-3}	-0.277978×10^{-3}
	Range of application: saturated liquid		
Temperature	−20 to 90°C	−20 to 90°C	−20 to 80°C

Table VIII. Coefficients in Eq. (7): $\lambda''(\vartheta) = d_0 + d_1\vartheta + d_2\vartheta^2$, with λ'' in $W \cdot m^{-1} \cdot K^{-1}$ and ϑ in °C

	R134a	R152a	R123
d_0	0.0122976	0.012282	0.0090054
d_1	0.293130×10^{-4}	0.77442×10^{-4}	0.527871×10^{-4}
d_2	0.175347×10^{-5}	0.96164×10^{-6}	0.440476×10^{-7}
	Range of application: saturated vapor		
Temperature	0 to 80°C	−20 to 80°C	30 to 90°C

saturation (λ'') states agree well at low temperatures, e.g., at the normal boiling point $\vartheta_{n.b.}$, but deviate from each other at higher temperatures. The curves for the saturated liquid and vapor are connected by a thin dotted line touching the critical isotherm ($\vartheta_{crit} = 101.1$°C). This line is meant to indicate the interconnection of the saturation lines; it is not, however, a suggested extrapolation, since both the thermal conductivity for liquid and that for vapor show steep peaks at the critical temperature [6].

Figure 5 also shows a comparison between the present R134a results and R12 curves as suggested by ASHRAE [26]. The thermal conductivity of R134a exceeds the respective R12 values in either case. The increase amounts to (i) 25 to 35% for saturated liquid, (ii) 40 to 70% for saturated vapor, and (iii) about 35% for vapor at ambient pressure.

In addition, our results are supplemented in Fig. 5 with some data available from the literature. Many thermal-conductivity measurements for R134a have been published within the last 4 years [13, 14, 18–25]. A comparison was made between all these measured data and the predictions according to our correlation in Eqs. (6) to (8). The deviations are shown in Fig. 6, where the temperature range is extended (-120°C $\leqslant \vartheta \leqslant +120$°C) to check for an extrapolation of our equations.

- For the saturated liquid (λ'; top, Fig. 6), deviations between the data sets are small (mostly within ±3%) in the range below 40°C, but they increase substantially beyond this temperature. Especially, the data of Ruvinskii et al. [12], Heide [23], and Jelesni et al. [24] are found above ours, and Laesecke and co-workers' data [22] are below, whereas the results of Ross et al. [14] are in good agreement with Eq. (6) (within the ±1.6% bounds of uncertainty). R134a appears as a substance difficult to investigate at higher temperatures. Deviations in the positive range may be due to influences of natural convection (both

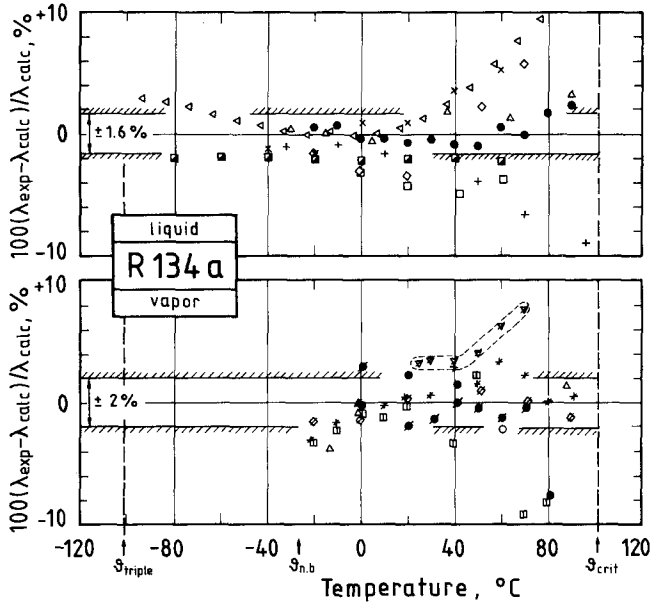

Fig. 6. Differences between measured and predicted thermal conductivities of R134a (for symbols see the key in Fig. 5).

Ruvinskii et al. [21] and Heide [23] applied steady-state methods with an increased risk of natural convection). Deviations may also arise if the transient hot-wire method is applied without precautions for the polarity of R134a. This has to be suspected in the case of Yata and co-workers' [19] and Kobayashi and co-workers' [20] experiments. Generally deviations in the positive direction have to be expected due to the critical enhancement within a temperature range of about $(\vartheta_{crit} - \vartheta) \leqslant 10\,K$.

- For the vapor at ambient pressure (λ_0) the deviations are generally small (within $\pm 2\%$); only Shankland and co-workers' results [18] deviate by a maximum of 8%.
- For the saturated vapor state (λ''), measurements are difficult and there are only a few data points in the literature. Most of the points presented in Fig. 5 are far away from saturation. Some of the literature results allow for an extrapolation to the saturation state. Such calculated values (not included in Fig. 5) are found to be in satisfactory agreement with Eq. (7).

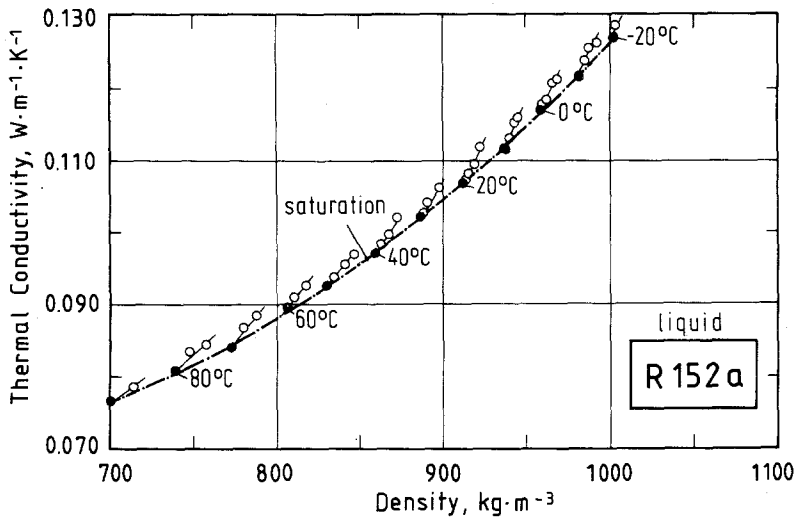

Fig. 7. Density and temperature effects on the thermal conductivity of R152a (liquid phase).

4.2. Thermal Conductivity of R152a

Measured thermal conductivities of R152a as presented in Figs. 7 and 8 show, again, the effects of density and temperature. Equation (4) and (5) can be fitted to the respective data sets with the coefficients listed in Tables V and VI.

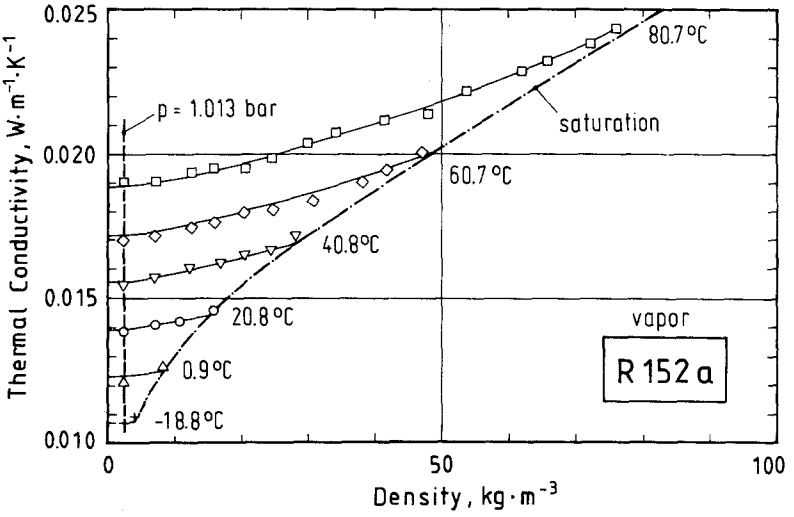

Fig. 8. Density and temperature effects on the thermal conductivity of R152a (vapor phase).

Figure 9 shows a diagram for the saturation and ambient-pressure thermal conductivities of R152a, which is similar to Fig. 5. The thermal conductivity λ'' of R152a in the saturated vapor state can be represented by almost the same curve as R134a in the saturated vapor state. The R152a saturated liquid thermal conductivity, on the other hand, exceeds that of R134a by 20 to 30%. The increase from R12 to R152a amounts to roughly 50% at lower temperatures (0°C) and to almost 80% at 80°C.

Our results are again compared with literature data [12, 23, 27–31] and the deviations from our correlation, Eqs. (6), (7), and (8), are plotted versus temperature in Fig. 10.

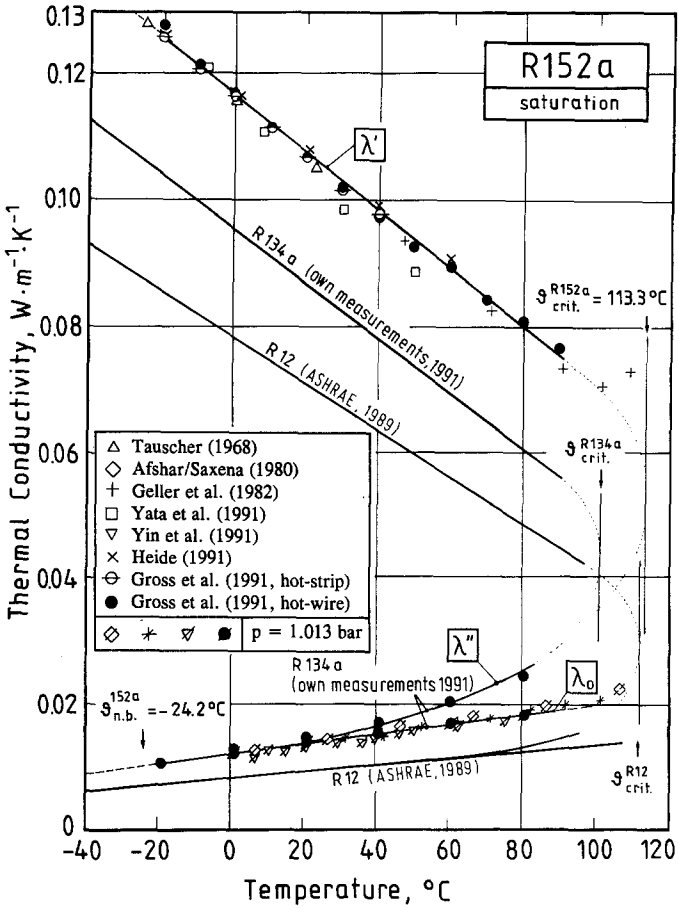

Fig. 9. Thermal conductivity of R152a in the saturated liquid and vapor states.

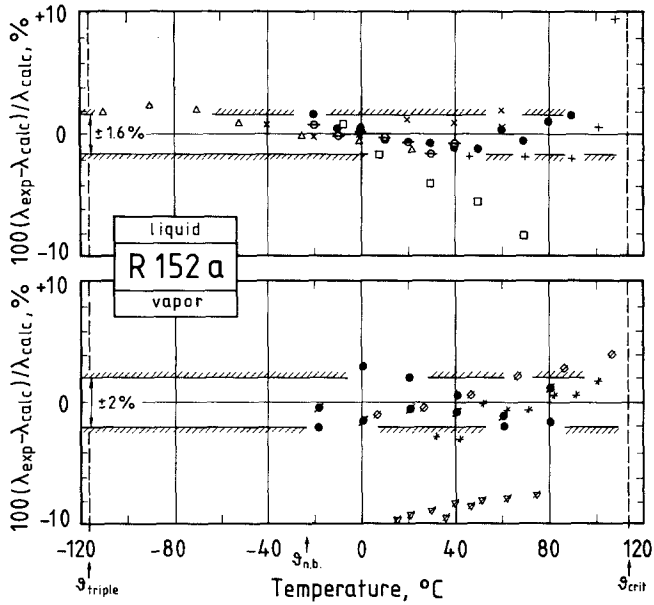

Fig. 10. Differences between measured and predicted thermal conductivities of R152a (for the symbols see the key in Fig. 9).

- The number of available data for saturated liquid R152a (λ') is much smaller than for R134a. Almost all results are predicted by Eq. (6) within $\pm 2\%$. This holds even for Tauscher's data [27] in the low-temperature range. Larger deviations (up to 9%) are found only for Yata and co-workers' results [30]. One point by Geller et al. [29] at $(\vartheta_{crit} - \vartheta) < 5$ K indicates the presence of a critical enhancement. The authors of the present paper performed additional measurements of liquid R152a thermal conductivity by means of the transient hot-strip method [12]. The principles of both methods, hot strip and hot wire, are similar, but the respective theories and the procedures of data evaluation are different. Thus they can be considered independent of each other. The results obtained by both methods are in good agreement.
- Comparison for the vapor state is possible only at ambient pressure (λ_0), with deviations mostly within $\pm 2\%$. Only Yin and co-workers' results [31] deviate by -8 to -11%. No saturation data are reported in the literature.

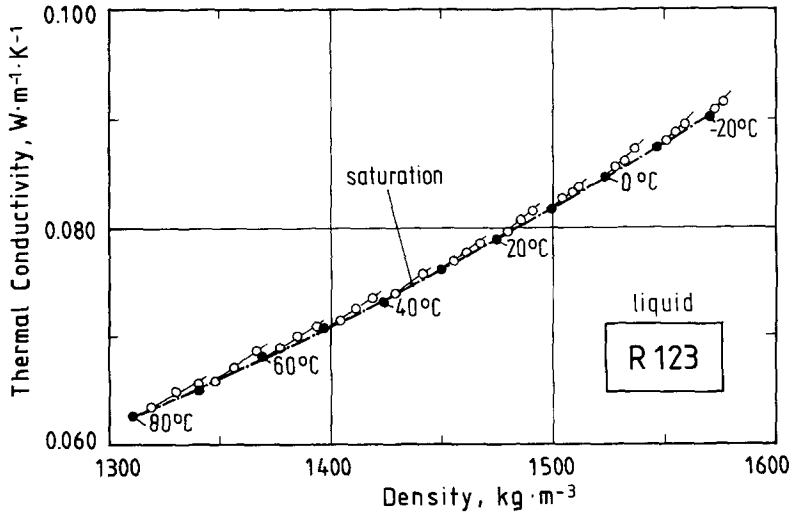

Fig. 11. Density and temperature effects on the thermal conductivity of R123 (liquid phase).

4.3. Thermal Conductivity of R123

Figures 11–14 show the results of our R123 thermal conductivity measurements together with data from the literature [19, 20, 25, 32–35]. A comparison with R11 data [26] shows that R123 thermal conductivity is (i) smaller by about 15% for saturated liquid, (ii) but larger by 30% for vapor.

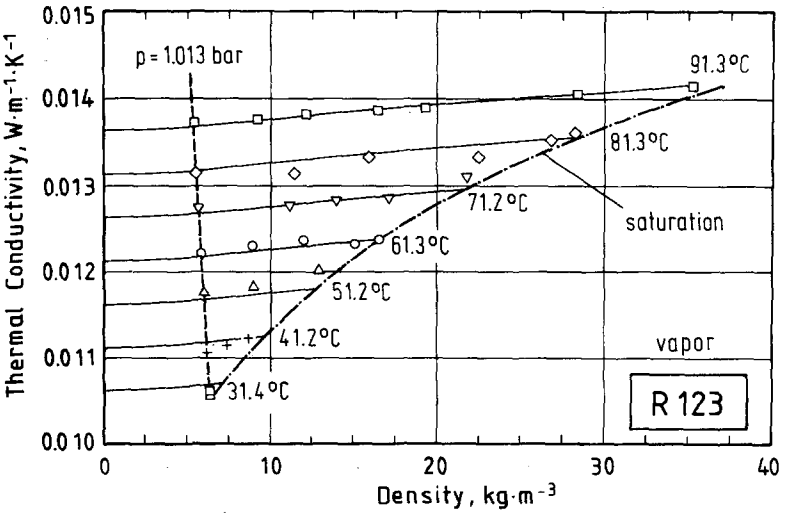

Fig. 12. Density and temperature effects on the thermal conductivity of R123 (vapor phase).

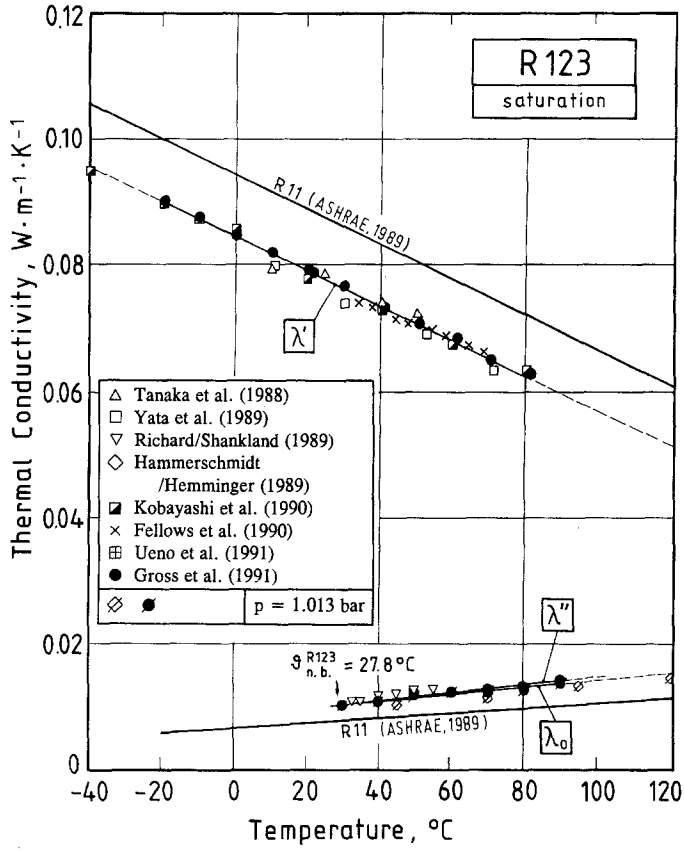

Fig. 13. Thermal conductivity of R123 in the saturated liquid and vapor states.

- In the saturated liquid state (λ'), almost all data in Fig. 13 agree with our correlation, Eq. (6), within $\pm 2\%$.
- The differences between the vapor data at ambient pressure (λ_0), Eq. (8), and at the saturation pressure (λ''), Eq. (7), are predominantly very small as shown in Fig. 14. This is due to the large distance from the critical point. There are, however, two data sets [33, 34] which show significant deviations from our measurements. The results measured by Richard and Shankland [33] for λ'' are found to be larger by 3 to 8%, just as for R134a [18], while those measured by Hammerschmidt and Hemminger [34] for λ_0 are smaller. The latter experiments were carried out

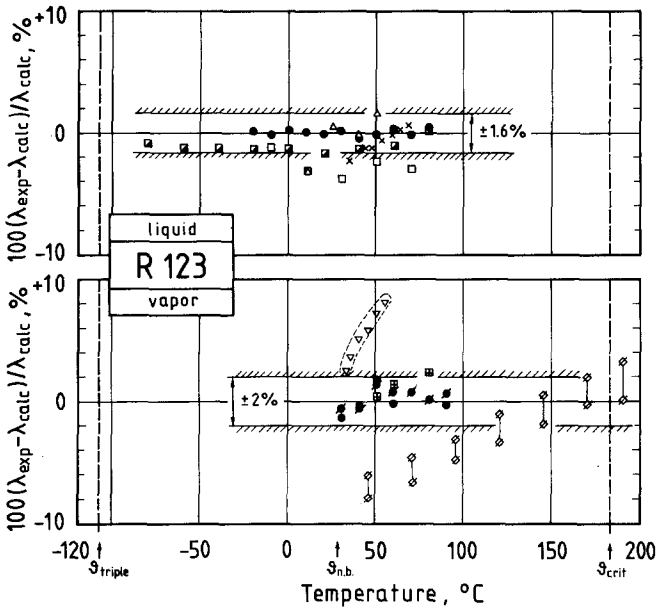

Fig. 14. Differences between measured and predicted thermal conductivities of R123 (for the symbols see the key in Fig. 13).

with a steady-state horizontal-plate method and an effect of sample thickness has been obtained. Therefore two deviations are given in Fig. 14 for each temperature: the upper one for a thickness $\delta = 1$ mm and the lower one for $\delta = 0.5$ mm. Our measurements and those by Hammerschmidt and Hemminger for high temperatures can be fitted well by Eqs. (7) and (8), within 2%.

5. EQUATIONS FOR PRACTICAL APPLICATIONS

For practical calculations the following equations are suggested.

5.1. Vapor at Ambient Pressure

Equation (8): $\lambda_0 = b_0 + b_1 \vartheta$, with the coefficients listed in Table VI

Range of application: $\vartheta_{n.b.} \leqslant \vartheta \leqslant 90°C$ for all three substances

This equation allows for an extrapolation to higher temperatures without large uncertainties.

5.2. Saturated Vapor

Equation (7): $\lambda'' = d_0 + d_1\vartheta + d_2\vartheta^2$,
with the coefficients listed in Table VIII

Ranges of application:

$0°C \leqslant \vartheta \leqslant 80°C$	for	R134a
$-20°C \leqslant \vartheta \leqslant 80°C$	for	R152a
$30°C \leqslant \vartheta \leqslant 90°C$	for	R123

Extrapolation of Eq. (7) is prohibited. Equation (8), however, can be applied for the calculation of saturated-vapor thermal conductivities at lower temperatures, even in the case of $\vartheta < \vartheta_{n.b.}$, without larger uncertainties, which might be due to extrapolation outsides the actual range of applicability of Eq. (8).

5.3. Saturated Liquid

Equation (6): $\lambda' = c_0 + c_1\vartheta$, with the coefficients listed in Table VII

Range of application: $-20°C \leqslant \vartheta \leqslant 90°C$ for all three substances

Extrapolation to higher temperatures is prohibited, but it is allowed to lower temperatures ($\vartheta < -20°C$).

ACKNOWLEDGMENTS

This investigation has been supported by the German Bundesministerium für Forschung und Technologie (BMFT). It is part of the New Refrigerants Research Program of the Deutscher Kältetechnischer Verein (DKV). Mr. J. Kellenbenz has contributed with his skill in data evaluation.

NOMENCLATURE

a	Thermal diffusivity
a_i, b_i, c_i, d_i	Coefficients
c_p	Isobaric specific heat capacity
d_i	Inner diameter
Q_1	Heat flux per unit length
p	Pressure
r	Radius
T, T_0	Thermodynamic temperature (at time zero)
t	Time
δ	Thickness
ϑ	Celsius temperature

λ	Thermal conductivity
λ_0	In the ideal-gas state
λ'	In the saturated-liquid state
λ''	In the saturated-vapor state
ρ	Density

Subscripts

crit	Critical point
n.b.	Normal boiling point ($p = 1.013$ bar)
triple	Triple point
w	Wire

REFERENCES

1. J. J. de Groot, J. Kestin, and H. Sookiazian, *Physica* **75**:454 (1974).
2. C. A. Nieto de Castro, J. C. G. Calado, W. A. Wakeham, and M. Dix, *J. Phys. E Sci. Instr.* **99**:1073 (1976).
3. J. J. Healy, J. J. de Groot, and J. Kestin, *Physica* **82C**:392 (1976).
4. H. M. Roder, *J. Res. NBS* **86**:457 (1981).
5. Y. M. Song, J. L. Lu, and S. Y. Fu, *Chinese J. Sci. Instr.* **6**:369 (1985).
6. E. Hahne, U. Gross, and Y. M. Song, *Int. J. Thermophys.* **10**:687 (1989).
7. E. Hahne and Y. W. Song, *Wärme- Stoffübertragung* **24**:79 (1989).
8. U. Gross, Y. W. Song, J. Kallweit, and E. Hahne, in *Proc. IIF/IIR Comm. B1 Meet., Herzlia/Israel* (1990), p. 103.
9. E. Hahne, Y. W. Song, and U. Gross, in *Convective Heat and Mass Transfer in Porous Media*, S. Kakac, ed. (Kluver Academic, Dordrecht, 1991), pp. 849–865.
10. U. Gross, Y. W. Song, J. Kallweit, and E. Hahne, *Energieträger Wasserstoff* (VDI-Verlag, Düsseldorf, 1991), pp. 234–255.
11. Y. W. Song, U. Gross, and E. Hahne, *Fluid Phase Equil.* (in press).
12. U. Gross, Y. W. Song, and E. Hahne, *Fluid Phase Equil.* **76**:273 (1992).
13. U. Gross, Y. W. Song, J. Kellenbenz, and E. Hahne, in *DKV-Tagungsbericht/Berlin* **18**(II/1):239 (1991).
14. M. Ross, J. P. M. Trusler, W. A. Wakeham, and M. Zalaf, in *Proc. IIF/IIR Comm. B1 Meet., Herzlia/Israel* (1990), p. 89.
15. T. Makita, ed., *Thermophysical Properties of Environmentally Acceptable Fluorocarbons HFC-134a and HFC-123* (Jap. Assoc. Refrig., Tokyo, 1990).
16. W. Blanke and R. Weiss, *Fluid Phase Equil.* (in press).
17. A. Kamei, C. C. Piao, H. Sato, and K. Watanabe, *ASHRAE Trans.* **96**(1):141 (1990).
18. I. R. Shankland, R. S. Basu, and D. P. Wilson, in *Proc. IIF/IIR Comm. B1, B2, E1, E2 Meet., Purdue* (1988), p. 305.
19. J. Yata, C. Kawashima, M. Hori, and T. Minamiyama, in *Proc. 2nd Asian Thermophys. Prop. Conf., Sapporo* (1989), p. 201.
20. Y. Kobayashi, Y. Ueno, Y. Nagasaka, and A. Nagashima, *High Temp.-High Press.* (in press).
21. G. Y. Ruvinskii, G. K. Larrenchenko, and S. V. Ilyushenko, *Kholodiln. Tekh.* 7:20 (1990).
22. A. Laesecke, R. A. Perkins, and C. A. Nieto de Castro, *Fluid Phase Equil.* (in press).

23. R. Heide, Private communication (1991).
24. W. P. Jelesni, L. D. Ljasota, M. D. Polapow, and D. A. Wladimorov, *Kholodiln. Tekh.* No. 7 (1991).
25. Y. Ueno, Y. Nagasaka, and A. Nagashima, *Proc. 12th Jap. Symp. Thermophys. Prop.* (1991), p. 225.
26. ASHRAE, *ASHRAE—Handbook Fundamentals* (ASHRAE Inc., Atlanta, Ga., 1989), Chap. 17.
27. W. A. Tauscher, *Kältetechnik-Klimatisierung* **20**:287 (1968).
28. R. Afshar and S. C. Saxena, *Int. J. Thermophys.* **1**:51 (1980).
29. V. Z. Geller, G. V. Zaporozhan, and S. V. Ilyushenko, *Prom. Teplotekh.* **4**(3):77 (1982).
30. J. Yata, M. Hori, T. Kurahashi, and T. Minamiyama, *Fluid Phase Equil.* (in press).
31. J. M. Yin, J. X. Guo, Z. Y. Zhao, L. C. Tan, and M. Zhao, *Fluid Phase Equil.* (in press).
32. Y. Yanaka, A. Miyake, H. Kashiwaga, and T. Makita, *Int. J. Thermophys.* **9**:465 (1988).
33. R. G. Richard and I. R. Shankland, *Int. J. Thermophys.* **10**:673 (1989).
34. J. Hammerschmidt and W. Hemminger, *DKV-Tagungsbericht/Hannover* **16**(2):397 (1989).
35. B. R. Fellows, R. G. Richard, and I. R. Shankland, in *Thermal Conductivity 21*, C. T. Cremmers and A. Fine, eds. (Plenum Press, New York, 1990).